ADVANCED OPTICAL MATERIALS
www.advopticalmat.de

Plasmon-Tunable Tip Pyramids: Monopole Nanoantennas for Near-Field Scanning Optical Microscopy

Thiago L. Vasconcelos, Bráulio S. Archanjo, Bruno S. Oliveira, Rogério Valaski, Rafael C. Cordeiro, Helton G. Medeiros, Cassiano Rabelo, Aroldo Ribeiro, Peter Ercius, Carlos A. Achete, Ado Jorio, and Luiz Gustavo Cançado*

Squeezing optical fields into nanometer scale is the key step to perform spatially resolved near-field optics. In scattering-type near-field optical microscopy, this task is accomplished by nanoantennas that convert propagating radiation to local near-fields and vice versa. The usual nanoantenna is composed by an elongated metal structure whose longitudinal dimension is scaled to support dipole modes of localized surface plasmon resonances. However, monopole modes can also be explored if the elongated metal nanoparticle is electrically grounded on a flat metallic plateau that acts like a mirror providing the monopole's image that closes the dipole system. Here, a method for batch production of monopole nanoantennas for scattering-type near-field scanning optical microscopy is presented. The nanoantennas are composed of a micropyramidal body with a nanopyramidal end whose lateral dimension can be scaled to fine-tune localized surface plasmon resonance modes. The monopole character of the nanoantennas is revealed by electron energy loss spectroscopy, and their efficiency and reproducibility are tested in tip-enhanced Raman spectroscopy experiments performed on single-layer graphene and single-walled carbon nanotubes.

Dr. T. L. Vasconcelos, Dr. B. S. Archanjo, B. S. Oliveira, Dr. R. Valaski, Dr. R. C. Cordeiro, H. G. Medeiros, Prof. C. A. Achete
Divisão de Metrologia de Materiais
Instituto Nacional de Metrologia Qualidade e Tecnologia (INMETRO)
25250-020 Duque de Caxias, RJ, Brazil
E-mail: tlvasconcelos@inmetro.gov.br

H. G. Medeiros
Polo Xerém
escola de Nanotecnologia
Universidade Federal do Rio de janeiro
21941-972 Rio de Janeiro, RJ, Brazil

C. Rabelo, A. Ribeiro, Prof. A. Jorio, Prof. L. G. Cançado
Departamento de Física
Universidade Federal de Minas Gerais
30270-901 Belo Horizonte, MG, Brazil

C. Rabelo
Graduate Program in Electrical Engineering
Universidade Federal de Minas Gerais
Av. Antônio Carlos 6627, 31270-901 Belo Horizonte, MG, Brazil

Dr. P. Ercius
National Center for Electron Microscopy
Molecular Foundry
Lawrence Berkeley National Laboratory
1 Cyclotron Rd., Berkeley, CA 94720, USA

DOI: 10.1002/adom.201800528

The main challenge of near-field scanning optical microscopy (NSOM) is to provide adequate local field enhancement that allows sufficient contrast between near-field and far-field signals.[1] In scattering-type NSOM mediated by nanoantennas, the field enhancement may be provided by a combination of the lightning rod effect and localized surface plasmon resonance (LSPR), both of them taking place at the apex of a sharp metal tip.[2] The LSPR is a special type of plasmon resonance supported by nanostructures smaller than the wavelength of the coupled radiation field.[3] The spatial confinement on the subwavelength nanostructure's surface gives rise to LSPR modes with wavelength determined by its size, shape, and chemical composition.[4–6] Indeed, local field enhancement can be observed at the apex of modified metal tips due to the presence of LSPR modes whose energies can be tuned by scaling the tip morphology.[7] This approach has been recently applied to electrochemically etched gold tips on which single transversal grooves have been milled by focused ion beam (FIB).[7] The scale factor that tunes the LSPR modes in this case is the distance L between the FIB-milled groove and the tip apex, as illustrated in **Figure 1**. There are two main drawbacks in this process: first, FIB milling processes are usually expensive and time consuming. Second, it is difficult to obtain electrochemically etched gold or silver tips with reproducible shape. The latter has been recently surpassed by the template-stripped gold pyramid method, in which pyramidal-like cavities on silicon are used as molds for gold and silver micropyramids fabrication.[8–10] These template-stripped pyramids (illustrated in Figure 1b) have been tested and proved to perform as efficient scattering-type near-field probes for tip-enhanced Raman spectroscopy (TERS)[11,12] and spatially resolved single-molecule photoluminescence.[11] The template-stripped method is beneficial for large-scale mass production, but the flat surface of the pyramid tip does not support LSPR modes in the visible range.

The field enhancement in the template-stripped pyramids is exclusively provided by the lightning rod effect, which means that this pyramidal system has never been tested at its full capacity. The maximum potential should be reached by adding a morphological barrier capable to generate LSPR. Here, we

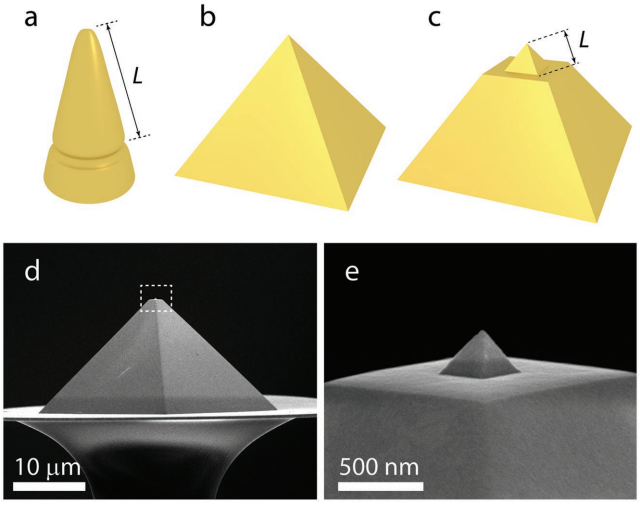

Figure 1. Illustrations of distinct types of nanoantennas used as scattering-type near-field metallic probes. a) FIB-milled electrochemically etched tip.[7] *L* is the distance between the milled groove and the apex, scalable to fine-tune LSPR modes. b) Template-stripped gold pyramid.[11] Its flat structure does not support LSPR in the visible range. c) Plasmon-tunable tip pyramid (PTTP) introduced in the present work. d,e) SEM images of a typical gold PTTP [(e) is a magnification of the boxed area in (d)]. This PTTP has an apex's diameter of ≈20 nm, and lateral edge length $L = 350$ nm.

introduce a method for mass-scale production of scattering-type near-field probes that combine the shape reproducibility of the template-stripped pyramids method with the high-field enhancement engendered by tunable LSPR modes. The method is based on a two-step lithography process that generates a micropyramidal body with a nanopyramid end, as illustrated in Figure 1c. The length L of the truncated nanopyramid tip is dimensioned to fine-tune LSPR modes, giving rise to a plasmon-tunable tip pyramid (PTTP). The localized surface plasmon (LSP) modes were studied by electron energy loss spectroscopy (EELS), and the results reveal that PTTPs act as monopole antennas, in contrast to the FIB-milled tips that present dipole behavior.[7] The monopole character of the PTTP is a consequence of its geometry: the nanopyramidal part is electrically grounded on a flat metallic plateau (Figure 1c–e) that acts like a mirror providing the monopole's image that closes the dipole system. Simulations based on the boundary element method (MNPBEM) were performed to determine a linear relation describing the resonance match between the PTTP length L and the wavelength of the coupled radiation field. The efficiency and reproducibility of the PTTPs were tested in TERS experiments[2,13] performed on single-layer graphene (SLG) and single-walled carbon nanotubes (SWCNT) samples as well-understood reference materials.[14,15] The results prove the realization of ultrahigh enhancement factor (in the order of 5100, as will be discussed later) with excellent yield (>90%).

The fabrication is similar to the template-stripped method,[11] with the difference that here the initial etching process is interrupted, and a second one takes place giving rise to the nanopyramid apex, as illustrated in Figure 1c. A detailed overview of the PTTP fabrication method is provided in the Supporting Information. The lateral length L is the key parameter, because it determines the effective wavelength of the LSPR modes supported by the PTTP, as discussed below. Figure 1d,e shows scanning electron microscopy (SEM) images of a typical gold PTTP produced by this method. The gold nanopyramid sitting on top of the flat plateau has an apex diameter of ≈20 nm, and lateral edge length $L \approx 350$ nm. Although we have used gold, the method can be adapted to other noble metals and alloys.

The quality and reproducibility of the produced cavities are inspected through SEM. This is an important step to assure that the PTTPs are shaped with the necessary structural parameters for LSPR tuning. A statistical analysis obtained from SEM inspection of 367 nanopyramidal cavities is presented in the Supporting Information. The distribution of lateral sizes of the base has a standard deviation smaller than 15% of the nominal size. This dimension is of great importance because it determines the effective wavelength of the LSPR modes supported by the PTTP, as discussed below. Another fundamental property of the nanopyramidal cavity is the shape of the bottom end, which determines the diameter of the PTTP apex and consequently the spatial resolution achieved in the near-field imaging process.[2] The statistical analysis revealed that the apex of the nanopyramidal cavities are smaller than 30 nm in 83% of the cases, and smaller than 50 nm for 93%. These numbers represent a relevant improvement on the reproducibility of relatively small tip apex sizes if compared to the conventional pyramids which, according to our analysis, present apex sharper than 50 nm in 12% of the analyzed cases (see details in the Supporting Information). As expected, the reduced size of the nanopyramid basis (few hundred of nanometers for the PTTPs, compared to 25 μm for conventional pyramids), leads to great improvement on the tip sharpness.

The plasmonic properties of the PTTPs were investigated by means of EELS performed inside of a transmission electron microscope.[7,16] EELS data cubes were extracted from PTTPs with $L = 350$ and 490 nm (see the Supporting Information). EELS spectra acquired at the vicinity of two PTTPs apexes are shown in **Figure 2**a. The raw data (solid lines) were deconvolved from the zero-loss peak point-spread function contribution by applying the Richardson–Lucy algorithm, which improves energy resolution and peak position accuracy.[17] The resulting deconvolved spectra are shown with dashed lines in Figure 2a. Both types of data (raw and deconvolved) clearly show two absorption peaks centered at 1.0 and 2.1 eV for the shorter nanopyramid ($L = 350$ nm), and at 0.8 and 1.7 eV for the longer one ($L = 490$ nm).

The influence of the geometrical parameter L on the absorption peak's energies indicates that the absorption processes originate from localized surface plasmon resonances. To confirm this hypothesis, we generated deconvolved EELS maps of the nanopyramids. The maps are shown in Figure 2b,c for the PTTPs with $L = 350$ and 490 nm, respectively. In both cases, the upper/bottom map is centered at the absorption peak with lower/higher energy (as observed in Figure 2a), within an energy window of 0.2 eV. For both PTTPs, the EELS map centered at the lower energy peak clearly shows only one strong hotspot localized in the vicinity of the nanopyramid apex. On the other hand, the plasmon absorption activity occurring at the highest energy peak is only observable in the EELS map extracted from the longest nanopyramid (bottom panel of Figure 2c). In this case, it is possible to observe two hotspots

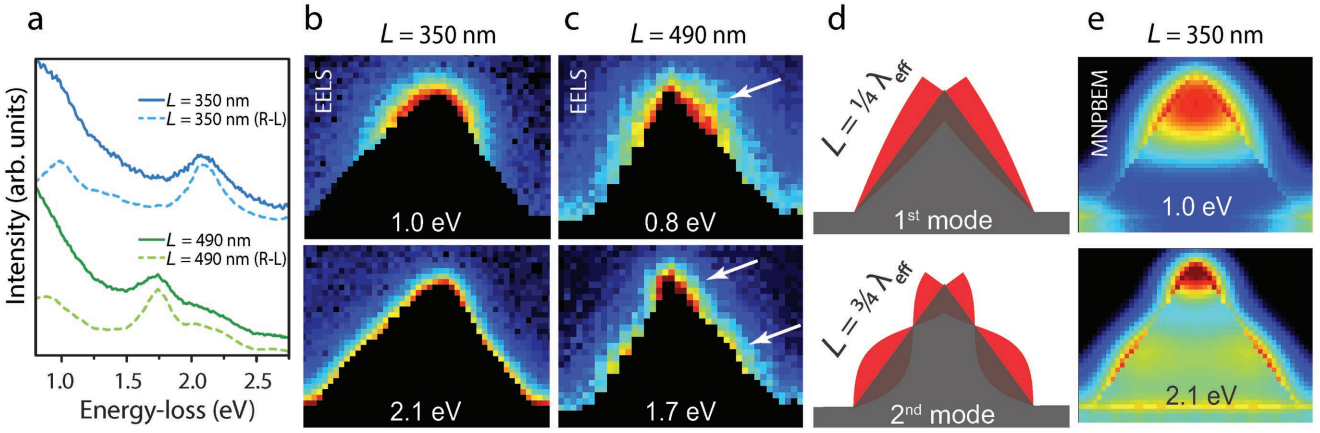

Figure 2. EELS and MNPBEM analysis of PTTP probes. a) EELS spectra acquired at the vicinity of two PTTPs nanopyramids with $L = 350$ nm (top-blue) and $L = 490$ nm (bottom-green). The raw data (solid lines) were deconvolved from the zero-loss peak point-spread function contribution by applying the Richardson–Lucy algorithm[17] resulting in the deconvolved spectra drawn with dashed lines. b,c) Deconvolved EELS maps of the nanopyramids with $L = 350$ nm and $L = 490$ nm, respectively. The upper and bottom maps are centered at 1.0 and 2.1 eV, respectively, in (b), and at 0.8 and 1.7 eV, respectively, in (c). The energy window is 0.2 eV in all cases. d) Illustration of the plasmonic behavior of the PTTPs. The top and bottom cartoons illustrate the first and second LSPR monopole modes occurring for $L = \frac{1}{4}\lambda_{\text{eff}}$ and $L = \frac{3}{4}\lambda_{\text{eff}}$, respectively. e) Reconstruction of the EELS maps obtained by MNPBEM simulations, considering a PTTP with $L = 350$ nm [same as in (b)]. As in (b)–(d), top and bottom maps reproduce the first and second modes, respectively.

(indicated by the white arrows), one located at the tip apex, the other located halfway from the apex to the base. This configuration indicates that PTTPs act as monopole antennas, as explained below.

An optical monopole antenna is formed by an elongated metal structure grounded in a metallic flat base. The elongated structure acts as one half of a dipole, or a monopole, with the other half being given by its image mirrored at the metallic base. Thus, monopole antennas support LSPRs whenever their lengths match odd multiples of $\lambda_{\text{eff}}/4$, λ_{eff} being the effective wavelength of the localized surface plasmon in the material system.[18] Figure 2d illustrates how this concept can be contextualized in the PTTP case. The PTTP is expected to act as a monopole antenna, since it is formed by an elongated structure (the nanopyramid) intrinsically connected to a metallic base (the plateau). The plateau acts as a mirror plane changing the dipole resonance of a freestanding nanopyramid to a monopole resonance.[19] The nanopyramid's base edges that interface with the plateau always hold minima of charge density variation, giving rise to resonances at odd multiples of $\lambda_{\text{eff}}/4$. Thus, the first and second LSPR modes occur for $L = \frac{1}{4}\lambda_{\text{eff}}$ and $L = \frac{3}{4}\lambda_{\text{eff}}$, respectively. The first and second monopole LSPR modes are illustrated in the top and bottom panels of Figure 2d, respectively. Notice how these monopole plasmon modes are analogous to longitudinal standing waves within a tube with a closed end (the base edge in the PTTP case).

In order to confirm that PTTPs hold the plasmonic properties of monopole antennas, we have performed MNPBEM simulations to reconstruct the EELS maps. The results for a PTTP with $L = 350$ nm are displayed in Figure 2e (top and bottom maps reproduce the first and second modes, respectively). The simulated maps are similar to the experimental results shown in Figure 2b,c, and they clarify the concept introduced in Figure 2d. A video provided in the Supporting Information shows 3D simulations of the first and second LSPR modes in a PTTP with $L = 350$ nm. The video shows how the hotspots of the second mode are concentrated at the nanopyramid's edges, which corroborates with the results reported in ref. [20]. It is worth to notice that no significant absorption peak is seen at the nanopyramid base, confirming its monopole nature.

We now focus on the optical properties of the PTTPs, adapting their geometry to produce effective probes for NSOM. In short, we must find the relationship between L and λ_{LSPR}—the wavelength of the incident radiation field that matches the resonance condition for LSPR. We keep our focus on the second LSPR mode because it provides better plasmonic confinement if compared to the first mode,[20] and the resonance occurs in the visible range for a feasible sized (not too short) PTTP nanopyramid. As clearly illustrated in Figure 2d, this resonance condition is satisfied for $L = \frac{3}{4}\lambda_{\text{eff}}$. The conventional antenna theory states that λ_{LSPR} equals λ_{eff} and therefore the characteristic length L of a monopole antenna equals $\frac{3}{4}\lambda_{\text{LSPR}}$ for the second mode. However, for a resonant nanoantenna working in visible range, λ_{LSPR} is distinct and generally larger than λ_{eff}. For gold or silver nanostructures, λ_{eff} is linearly related to λ_{LSPR} as $\lambda_{\text{eff}} = n_1 + n_2 \frac{\lambda_{\text{LSPR}}}{\lambda_{\text{p}}}$, where n_1 and n_2 are parameters that depend on the geometry and material properties of the antenna, and λ_{p} is the plasmon wavelength (for gold, $\lambda_{\text{p}} = 138$ nm).[4] This linear relation holds faraway from interband electron transitions, which occur at $\lambda \approx 560$ nm for gold.[4–6] Based on these grounds, the linear relation between the second LSPR mode's wavelength ($\lambda^{(2)}_{\text{LSPR}}$) and L was explored by means of MNPBEM simulations employed for PTTPs with $L = 300$, 350, 400, and 450 nm (see details in the Supporting Information). The results are shown in **Figure 3**a, which plots $\lambda^{(2)}_{\text{LSPR}}(\text{nm})$ as a function of L. The diamond symbols are the results obtained from the MNPBEM simulations, and the solid line is the result of a linear fit that yields $\lambda^{(2)}_{\text{LSPR}}(\text{nm}) = 335 + 0.69L(\text{nm})$. The EELS data originating

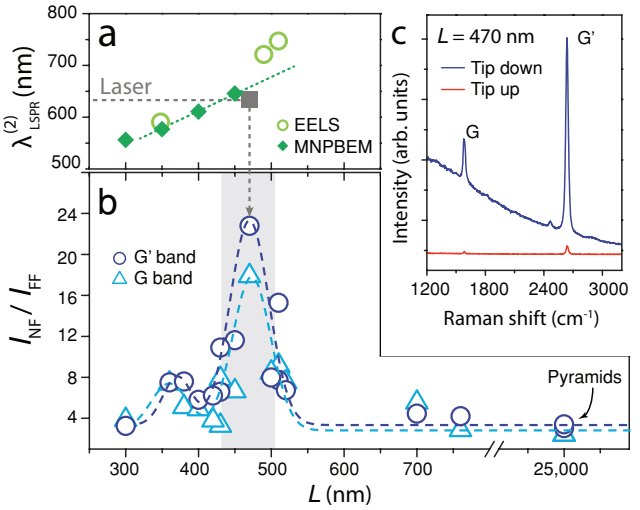

Figure 3. a) Plot of the second LSPR mode's wavelength ($\lambda^{(2)}_{LSPR}$) as a function of nanopyramid characteristic length L. The open circles are experimental EELS data. Diamond symbols are the results obtained from the MNPBEM simulations and the solid line is the result of a linear fit that yields $\lambda^{(2)}_{LSPR}(\text{nm}) = 335 + 0.69L(\text{nm})$. b) Tip-enhanced Raman data obtained from single-layer graphene. The vertical axis scales the ratio I_{NF}/I_{FF}, where I_{NF} is the integrated intensity of a Raman band obtained in the presence of the PTTP, and I_{FF} is the integrated intensity of the same Raman band obtained without the PTTP. The horizontal axis scales the PTTP characteristic length L. The data extracted from the G and G′ bands using distinct PTTPs are displayed as open triangles and circles, respectively. The data at L = 25 µm were obtained using a typical pyramid tip which, for practical terms, was considered as a PTTP with $L \gg \lambda_{LSPR}$. c) Two exemplary Raman spectra obtained from a SLG piece with (top-blue spectrum) and without (bottom-red spectrum) the PTTP. The PTTP has L = 470 nm which, according to the results shown in (b), provide the best condition for LSPR tuning.

from three distinct tips, including those showed in Figure 2, are plotted in the same graphic (open circles), showing a good agreement with the simulation data in the range of $L < 500$ nm.

To experimentally test the PTTPs' optical efficiency, 15 of them were produced with distinct characteristic lengths L, and applied in TERS experiments using a SLG as the reference sample. SLG is an excellent reference sample for a metrological TERS platform for the following reasons: (i) it has been previously measured in several works,[12,14,21,22] allowing the comparison between different NSOM probes and systems; (ii) it is simple to be obtained with good reproducibility;[12,23] (iii) it is suitable for an easier tip-sample-focus alignment.[14] The experimental setup used here is similar to that described in ref. [15], and the experiment was carried out using a HeNe laser source (λ = 632.8 nm). Figure 3b shows the results obtained for the TERS signal. The vertical axis is the I_{NF}/I_{FF}, where I_{NF} is the integrated intensity of a Raman band obtained in the presence of the PTTP (the NF subscript stands for near-field), and I_{FF} is the integrated intensity of the same Raman band obtained without the PTTP (FF stands for far-field). The horizontal axis scales the PTTP characteristic length L. The two main Raman features of pristine graphene were taken into account: the first-order bond stretching G mode, centered at ≈1580 cm^{-1}, and the two-phonon totally symmetric G′, also called 2D mode, centered at ≈2700 cm^{-1}. The values of I_{NF}/I_{FF} extracted from the G and G′ bands are displayed in Figure 3b as open triangles and circles, respectively. The data at L = 25 µm were obtained using a typical pyramid tip which, for practical terms, can be considered as a PTTP with $L \gg \lambda_{LSPR}$. Figure 3c shows two exemplary Raman spectra obtained from a SLG piece with (top spectrum) and without (bottom spectrum) the presence of the PTTP (L = 470 nm).

The experimental data plotted in Figure 3b reveal the occurrence of a clear resonance profile (inside the shaded area). The Gaussian fit to the experimental data (dashed lines) gives a resonance width of ≈50 nm, revealing a high-quality resonance factor (spectral position divided by the resonance peak width) $Q \approx 10$.[5] The maximum signal enhancement occurs for $L \approx 470$ nm.[24] This value was extended to the plot in Figure 3a, with $\lambda^{(2)}_{LSPR}$ set to 632.8 nm (the wavelength of the HeNe laser used in the experiment). The length L that provided the maximum enhancement in the TERS experiment is slightly larger (about 40 nm) than that predicted from the simulations MNPBEM. One possible explanation for this discrepancy is an overestimation of L, since the nanopyramid should be slightly smaller than the corresponding silicon cavity, from which L is actually measured.

The most important aspect of the experimental result shown in Figure 3b is related to the maxima values achieved for the I_{NF}/I_{FF} ratio, being ≈18 and 23 for the G and G′ bands, respectively. The G band is actually expected to present lower enhancement than the G′ due to interference effects occurring in the near-field regime.[12,25] Taking into account all geometrical factors (incident laser spot radius at the focal plane ≈275 nm, and tip apex radius ≈18 nm),[26] the enhancement factor can be estimated using a back-of-the-envelope calculation as $M = \left[\frac{I_{NF} - I_{FF}}{I_{FF}}\right] \times (A_{FF}/A_{NF})$, where A_{NF} and A_{FF} are the sample areas probed in the near-field (area under the tip) and far-field (focus area) regimes, respectively,[27] obtained for the G′ band is 5100 ± 230.[28] This value is one order of magnitude higher than typically achieved for ordinary gold pyramids (M = 460 ± 190 and M = 380 ± 230 for the pyramids tested in this work, and $I_{NF}/I_{FF} \approx 2.6$ or $M \approx 370$ for the data showed in ref. [12]). However, M can be highly misleading due to the use of unrealistic geometrical factors.

A robust comparison between the level of enhancement achieved by these two types of near-field probes is presented in **Figure 4**, which shows the plot of the I_{NF}/I_{FF} ratio related to the G′ band as a function of the distance between the tip apex and the graphene sample. The data used for pyramid were taken from ref. [12], where the experiment was performed under similar conditions [same sample system (SLG), similar setups, same HeNe laser source, probes made of gold]. Clearly, the signal enhancement achieved with the PTTP is much higher than that achieved with an ordinary pyramid. The solid lines are fit to experimental data following the theory proposed in refs. [12,25]. The analysis revealed a field enhancement factor of $f_e \approx 9$ for the PTTP, and ≈4.5 for the pyramid.[12] This enhancement factor is a measure of the tip polarizability's strength.[12,25] The actual Raman signal enhancement scales with f_e^4,[15] which is ≈6500 for the PTTP and ≈410 for the pyramid, in rough agreement with the back of the envelope calculation (M factor).[29] These values indicate that tuned PTTPs

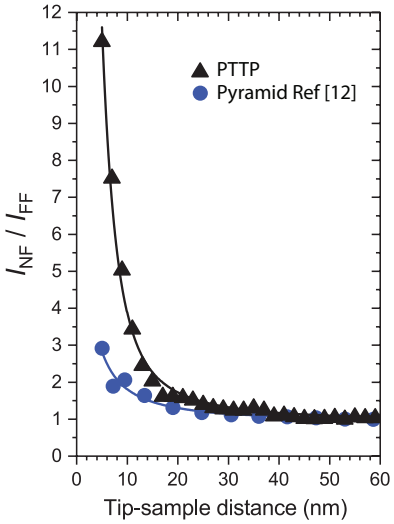

Figure 4. Plot of the I_{NF}/I_{FF} ratio related the G′ band as a function of the distance between the tip apex and the graphene sample. Triangles are experimental data obtained using a PTTP with $L = 470$ nm. Circles are experimental data obtained using ordinary pyramids, taken from ref. [12]. The solid lines are fits to the experimental data following the theory proposed in refs. [12,25].

generate extremely high and, to the best of our knowledge, unprecedented local field enhancement.

It has been previously shown that monopole antennas provide stronger LSPR than dipole ones,[19] and the reason is that the field pattern generated at the apex of the monopole antenna resembles the overlap of half of a fictitious freestanding dipole with the other half generated by the mirror plane. Therefore, this system should account for at least a fourfold higher enhancement factor for local field intensity. Another important factor is the polarization of the incident field. For better performance, we have used a radially polarized incident beam. This system presents a longitudinal polarization component at the focal plane, which becomes specially important for strongly focused fields obtained with objective lenses with high numerical apertures (NA). This longitudinal component presents the best configuration to excite localized surface plasmons along the nanopyramid shaft. On the other hand, the gold plateau located at hundreds of nanometers away from the focal plane is illuminated by a radially polarized field oriented parallel to its surface. Although the plateau may not be able to support localized surface plasmons, the radially polarized field certainly generates free-charge density oscillations at the same frequency as the incident radiation field. This collective motion of the electronic cloud inside of the gold plateau acts as an AC current source capable of enhancing the mirror effect that generates the monopole antenna.

The capability of the PTTPs to perform optical imaging with high spatial resolution was tested in the TERS schema. Compared to our previous experience, PTTPs considerably improve the feasibility of TERS imaging, providing much higher yield than any other NSOM probe we have tested before. **Figure 5**a shows the TERS image of a SWCNT, where the color scale renders the G band intensity. The image was obtained using a PTTP with $L = 470$ nm and HeNe laser as the light source. A lateral resolution of ≈10 nm was extracted from the full

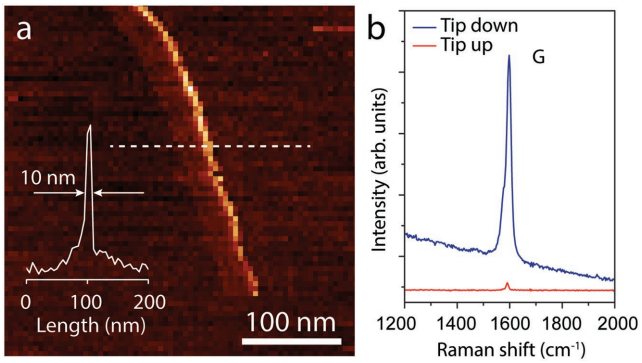

Figure 5. a) TERS image of a SWCNT obtained using a tuned PTTP ($L = 470$ nm and HeNe laser for incident illumination). The color scale renders the G band intensity. The inset shows the plot of the G band intensity profile taken along the dashed line crossing the nanotube. b) Raman spectra of the same SWCNT, acquired with the PTTP (indicated as tip down) and without the PTTP (indicated as tip up).

width at half maximum of the G band intensity profile (inset to Figure 5a) taken along a transversal line across the tube axis (white dashed line). Figure 5b shows two Raman spectra of the SWCNT, one acquired with the PTTP (indicated as tip down) and the other without the PTTP (indicated as tip up), giving rise to a signal enhancement of $I_{NF}/I_{FF} \approx 33$. A similar TERS experiment was performed on arc-discharge CNT bundles in ref. [11], using conventional gold pyramids and similar setups (although using 785 nm laser). The system achieved a signal enhancement of $I_{NF}/I_{FF} \approx 10$, with resolution of ≈33 nm.

In summary, PTTPs can be designed to provide highly efficient local field enhancement for scanning near-field optical microscopy. EELS measurements show that PTTPs act as monopole nanoantennas: the nanopyramid apex supports localized surface plasmon resonances whenever its characteristic length L matches odd multiples of $\lambda_{eff}/4$, being λ_{eff} the effective wavelength of the localized surface plasmon. The nanopyramid acts as one half of a dipole, the other half being given by its image mirrored at the metallic base. MNPBEM simulations were employed to reconstruct the EELS maps confirming its monopole behavior. The simulated data were also used to scale the PTTPs characteristic length L to the λ_{LSPR}. The PTTP optical efficiency was tested in TERS experiments, and the results show that the level of local field enhancement is approximately two orders of magnitude higher than the values typically achieved for ordinary gold pyramids[12] and FIB-milled gold tips.[7] The fabrication process is adequate for batch production with more than 90% yield.

Supporting Information

Supporting Information is available from the Wiley Online Library or from the author.

Acknowledgements

This work was supported by INMETRO, FAPERJ, CNPq (Grant No. 552124/2011-7), and FAPEMIG. Work at the Molecular Foundry was supported by the Office of Science, Office of Basic Energy Sciences,

of the U.S. Department of Energy. The authors thank Ryan Beams for critical reading of the manuscript.

Conflict of Interest

The authors declare no conflict of interest.

Keywords

electron energy loss spectroscopy, localized surface plasmon resonance, monopole nanoantennas, scanning near-field optical microscopy, tip-enhanced Raman spectroscopy

Received: April 20, 2018
Revised: June 22, 2018
Published online:

[1] T. X. Huang, S. C. Huang, M. H. Li, Z. C. Zeng, X. Wang, B. Ren, *Anal. Bioanal. Chem.* **2015**, *407*, 8177.
[2] X. Shi, N. Coca-López, J. Janik, A. Hartschuh, *Chem. Rev.* **2017**, *117*, 4945.
[3] S. A. Maier, *Plasmonics: Fundamentals and Applications*, Springer Science & Business Media, New York **2007**.
[4] L. Novotny, *Phys. Rev. Lett.* **2007**, *98*, 266802.
[5] L. Novotny, N. Van Hulst, *Nat. Photonics* **2011**, *5*, 83.
[6] P. Biagioni, J. Huang, B. Hecht, *Rep. Prog. Phys.* **2012**, *75*, 24402.
[7] T. L. Vasconcelos, B. S. Archanjo, B. Fragneaud, B. S. Oliveira, J. Riikonen, C. Li, D. S. Ribeiro, C. Rabelo, W. N. Rodrigues, A. Jorio, C. A. Achete, L. G. Cançado, *ACS Nano* **2015**, *9*, 6297.
[8] J. Henzie, E. S. Kwak, T. W. Odom, *Nano Lett.* **2005**, *5*, 1199.
[9] P. Nagpal, N. C. Lindquist, S.-H. Oh, D. J. Norris, *Science* **2009**, *325*, 594.
[10] N. C. Lindquist, T. W. Johnson, P. Nagpal, D. J. Norris, S.-H. Oh, *Sci. Rep.* **2013**, *3*, 1857.
[11] T. W. Johnson, Z. J. Lapin, R. Beams, N. C. Lindquist, S. G. Rodrigo, L. Novotny, S. H. Oh, *ACS Nano* **2012**, *6*, 9168.
[12] R. Beams, L. G. Cançado, S. H. Oh, A. Jorio, L. Novotny, *Phys. Rev. Lett.* **2014**, *113*, 1.
[13] P. Verma, *Chem. Rev.* **2017**, *9*, 6447.
[14] R. Beams, *J. Raman Spectrosc.* **2018**, *49*, 157.
[15] L. G. Cançado, A. Hartschuh, L. Novotny, *J. Raman Spectrosc.* **2009**, *40*, 1420.
[16] O. Nicoletti, F. de la Peña, R. K. Leary, D. J. Holland, C. Ducati, P. a. Midgley, *Nature* **2013**, *502*, 80.
[17] E. P. Bellido, D. Rossouw, G. a. Botton, *Microsc. Microanal.* **2014**, *20*, 767.
[18] T. H. Taminiau, R. J. Moerland, F. B. Segerink, L. Kuipers, N. F. van Hulst, *Nano Lett.* **2007**, *7*, 28.
[19] S. Li, W. Zhou, D. B. Buchholz, J. B. Ketterson, L. E. Ocola, K. Sakoda, P. H. Chang, *Appl. Phys. Lett.* **2015**, *104*, 231101.
[20] B. S. Archanjo, T. L. Vasconcelos, B. S. Oliveira, C. Song, F. Allen, C. A. Achete, P. Ercius, *ACS Photonics* **2018**, *5*, 2834.
[21] W. Su, D. Roy, *J. Vac. Sci. Technol. B* **2013**, *31*, 41808.
[22] R. Beams, L. G. Cançado, A. Jorio, A. N. Vamivakas, L. Novotny, *Nanotechnology* **2015**, *26*, 175702.
[23] Y. Huang, E. Sutter, N. N. Shi, J. Zheng, T. Yang, D. Englund, H. J. Gao, P. Sutter, *ACS Nano* **2015**, *9*, 10612.
[24] It should be noticed the presence of an additional, and considerably lower, peak in Figure 30b, occurring at $L \approx 370$ nm. There are two hypotheses for the origin of this peak. The first and most probable is that it is related to the first dipole LSPR mode. Although the nanopyramid is obviously grounded to the plateau, the edges of its basis might present enough perturbation to trap dipole modes of localized surface plasmons. The second hypothesis would be the broadening of the LSPR monopole resonance peak when approaching energies close to the interband transition threshold.[30] This damping effect becomes important when $\lambda_{LSPR}^{(2)} \approx 560$ nm, the wavelength associated with the 5d-6sp interband transition in gold.
[25] L. G. Cançado, R. Beams, A. Jorio, L. Novotny, *Phys. Rev. X* **2014**, *4*, 31054.
[26] The radius of the focal plane is defined by the Rayleigh criterion ($r_{focus} = 0.61\ \lambda_L/NA$, with $\lambda_L = 632.8$ nm, and NA = 1.4).[27,31] The value of the tip apex radius was extracted from the intensity profile of the disorder-induced D band (≈1350 cm^{-1}) obtained by scanning the sharp edge of a graphene sample (same method as in ref. [12]).
[27] J. Stadler, T. Schmid, R. Zenobi, *Nanoscale* **2012**, *4*, 1856.
[28] The error for this method can be estimated to be A_{FF}/A_{NF}.[31]
[29] The field enhancement factor (f_e) and the signal enhancement factor (M) are related to each other as: $M \approx f_e^2(\omega_i) f_e^2(\omega_s) \sim f_e^4(\omega_i)$, where ω_i is the frequency of the incident light, and ω_s is the frequency of the scattered light.[15]
[30] C. Sönnichsen, T. Franzl, T. Wilk, G. von Plessen, J. Feldmann, O. Wilson, P. Mulvaney, *Phys. Rev. Lett.* **2002**, *88*, 77402.
[31] N. Kumar, A. Rae, D. Roy, N. Kumar, A. Rae, D. Roy, *Appl. Phys. Lett.* **2014**, *104*, 123106.

